CALIFORNIA INSTITUTE OF TECHNOLOGY

Hydrodynamics Laboratories

THE HYDRODYNAMICS OF THE FREE-SURFACE WATER TUNNEL

A REPORT ON RESEARCH CONDUCTED UNDER CONTRACT WITH
THE BUREAU OF ORDNANCE OF THE DEPARTMENT OF THE NAVY

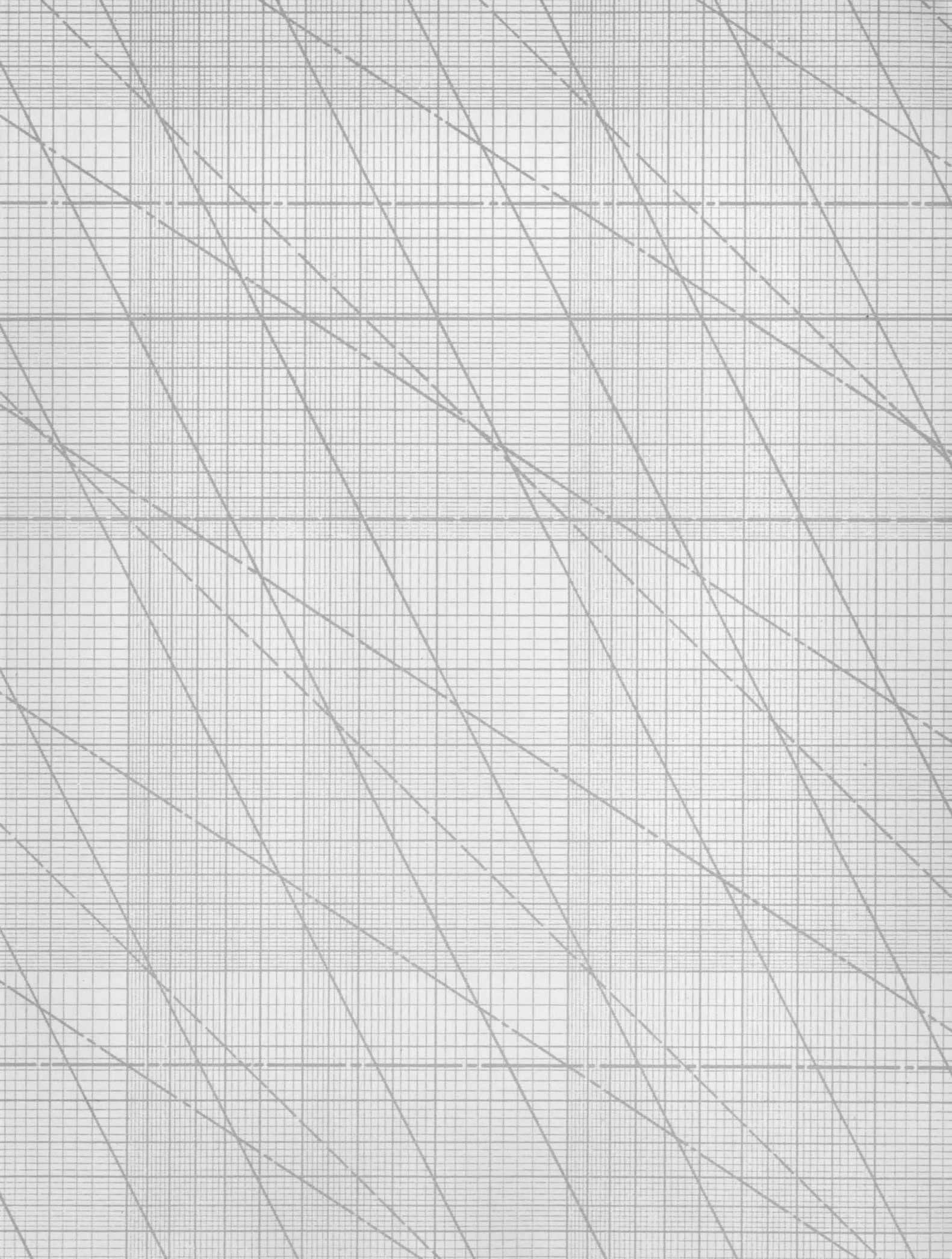

DYNAMIC SIMILITUDE NEAR AN AIR-WATER INTERFACE

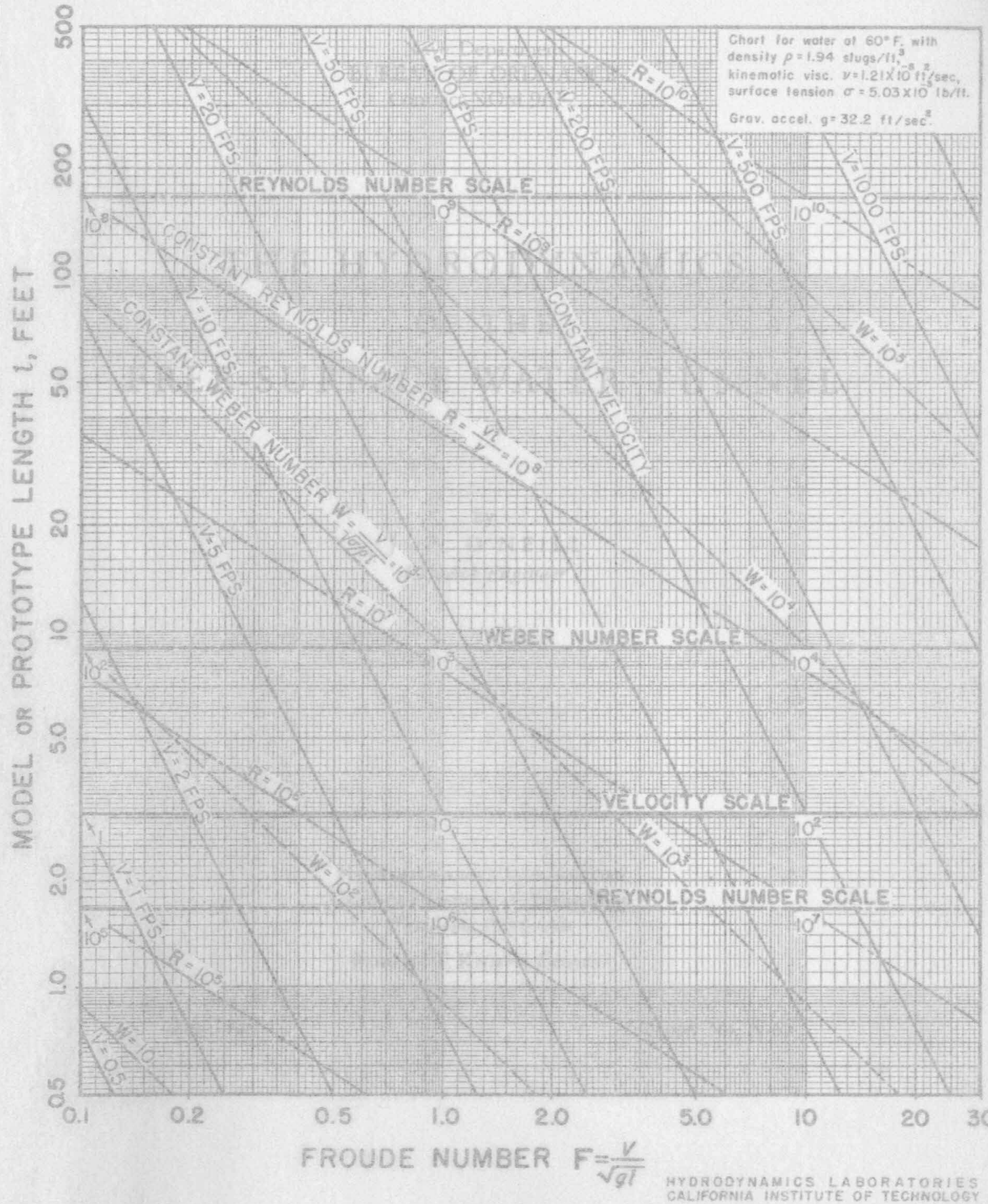

HYDRODYNAMICS LABORATORIES
CALIFORNIA INSTITUTE OF TECHNOLOGY

Navy Department
BUREAU OF ORDNANCE
Contract NOrd 9612

THE HYDRODYNAMICS OF THE FREE-SURFACE WATER TUNNEL

by
J. P. O'NEILL
Research Engineer

HYDRODYNAMICS LABORATORY
California Institute of Technology
Pasadena, California
ROBERT T. KNAPP, *Director*

May 1949 *Report No. N-65*

TABLE OF CONTENTS

THE HYDRODYNAMICS OF THE FREE-SURFACE WATER TUNNEL

ABSTRACT

Free-surface water tunnels are used to determine the hydrodynamic characteristics of bodies which move in water near the surface. To develop the basic principles for the design and operation of such a tunnel the conditions for dynamic similitude near an air-water interface are analyzed. Although the tests should determine how the hydrodynamic characteristics are affected by the surface waves produced by the body itself, the dimensions and conditions of operation of the test channel are sometimes responsible for disturbances that interfere with the interpretation of the local wave effect. In order to record the type of interfering waves that might be expected and the conditions responsible for their occurrence, the Free-Surface Water Tunnel at the Hydrodynamics Laboratory of the California Institute of Technology was temporarily operated under these conditions. Since the local wave pattern produced by the body under study depends primarily on the criterion for inertial-to-gavitational similitude between model tests and prototype operation, the relation between this criterion and the conditions that produce the undesirable channel waves is discussed.

Application of gravitational similitude usually results in model tests that are different from prototype operation in respect to viscous and surface-tension effects. A chart is developed showing the relations for gravitational similitude and indicating the resulting dissimilitude for viscous and surface-tension phenomena. This chart is also used to indicate the complete range of operation of a free-surface test channel as well as the range in which undesirable waves are produced in the working section. Through recognition of the nature of the interactions between the hydrodynamic characteristics of the tunnel and the body under investigation, design and operation principles for a free-surface water tunnel are developed showing how to decrease or avoid the wave difficulties and minimize the unavoidable dissimilitude.

THE HYDRODYNAMICS OF THE FREE-SURFACE WATER TUNNEL

Introduction

Difficulties are usually encountered when the velocity of propagation of waves in a fluid is about equal to the velocity of the fluid relative to the boundaries. Because of these difficulties there has been some surprise at the orderly behavior during normal operation of the Free-Surface Water Tunnel at the Hydrodynamics Laboratory.[1] The tunnel provides the relative fluid motion and the mechanism for propagation of waves since its function is to get a stream of flowing water in which bodies may be supported for determining their hydrodynamic characteristics when in close proximity to the water surface. A wide and active interest in wave phenomena similar to those that occur in this tunnel has resulted in considerable discussion of the flow problems dealt with during its design and operation. Requests for information on methods of dealing with these flow problems and for comments on proposed tunnels of this type have shown a need for the formulation of the fundamental hydraulic principles that might be used as a guide for the design and use of a free-surface water tunnel. The principles that appear most fundamental have been formulated from the laws of dynamic similitude near an air-water interface.

The very feature that is the distinguishing characteristic of a free-surface water tunnel is responsible for most of the difficulties in its operation. Surface waves are produced when a test object intersects or is near an interface between two fluids and is in motion relative to one or both of the fluids. The hydrodynamic forces on the body under test are influenced by the shape of the waves produced by the body itself since this distorted interface becomes part of the boundary of the flow pattern. The purpose of tests in a free-surface water tunnel is to find out how the hydrodynamic forces are affected by this wave shape that is produced by the local disturbance alone; the surface contours throughout the open channel of the tunnel are determined, however, by the channel boundaries as well as the disturbance produced by the body under test. As a consequence of the influence of the channel boundaries, it may be difficult to interpret the local wave effect; furthermore, under some conditions, this influence may determine the wave shape to such an extent that the desired tunnel-operating conditions cannot be obtained. During the design and use of a free-surface water tunnel, it is therefore necessary to consider the behavior of surface waves as affected by both the local disturbance and the channel dimensions.

[1] "The Hydrodynamics Laboratory of the California Institute of Technology," by R. T. Knapp, Joseph Levy, J. P. O'Neill, and F. B. Brown; Trans. ASME, Vol. 70, No. 5, 1948, pp. 437-457.

The Froude Number of a Model or Prototype

Where an interface between two fluids of different specific weight forms part of the boundary of a flow pattern, the form of the interface is determined predominantly by the ratio of the inertial force per unit volume due to the motion of the fluids relative to the solid boundaries, and the gravitational force per unit volume due to the difference in the specific weights. When relative motion of only one of the fluids is significant, the ratio is proportional to

$$\frac{\rho V^2/l}{\Delta\gamma}$$

where V is the velocity of the significant relative motion, ρ is the density of the fluid having this motion, l is a characteristic length, and $\Delta\gamma$ is the difference in the specific weights of the two fluids.* The square root of this dimensionless parameter gives the Froude number in the form

$$\mathbf{F} = \frac{V}{\sqrt{l\Delta\gamma/\rho}} . \qquad (1)$$

Furthermore, when the specific weight of one fluid is very much smaller than the other, as when water and air are involved, $\Delta\gamma$ is almost equal to the specific weight γ of water. Then, since γ/ρ is equal to the gravitational acceleration g, the Froude number reduces to

$$\mathbf{F} = \frac{V}{\sqrt{gl}} . \qquad (2)$$

The ratio in this form is a sufficient criterion to determine the contour of any gravity wave that acts as part of the boundary of a steady-state flow pattern in water when air is above the interface and the predominant forces are those of inertia and gravity. The Froude number consequently determines the behavior of gravity waves resulting from the presence of a test object or model supported in a free-surface water tunnel and, when l is a characteristic length of a model or prototype, it is

* The relative motion of only one of the fluids is significant when ρV^2 for one is much greater than for the other. This condition prevails for the usual velocities involved when air and water are the two fluids. The Newtonian relationship for fluid acceleration gives the inertial force per unit volume of water $f_i = \rho a$ where the acceleration $a = dv/dt$. If this volume of water having the mass ρ moves a distance s, its velocity is $v = ds/dt$. Then, since $dt = ds/v$, $f_i = \rho v dv/ds = (1/2)\rho d(v^2)/ds$, i.e., the inertial force per unit volume $f_i \propto \rho V^2/l$. The gravitational force per unit volume of water is due to its specific weight γ_w; by Archimedes principle, however, the water is supported by a hydrostatic force equal to the weight γ_a of the displaced air. The net gravitational force on a unit volume of water is consequently the difference in their specific weights $\Delta\gamma$.

the criterion for similitude between model tests and prototype operation.

The Froude Number of the Free-Surface Test Channel

Any possible steady-state flow pattern that is affected by the channel dimensions in a free-surface water tunnel can be described as a function of the Froude number using the depth of flow y as the length parameter. This Froude number is consequently the criterion for evaluation of the wave effect previously mentioned which might interfere with the operation of the tunnel or with the determination of what part of the measured hydrodynamic forces on a test body are the result of the surface waves created by the body. The numerical value of this channel Froude number

$$\mathbf{F}_y = \frac{V}{\sqrt{gy}} \tag{3}$$

is significant as the ratio of the velocity of flow to the celerity

$$C = \sqrt{gy} \tag{4}$$

of an elementary gravity wave having a long wave length and small amplitude compared with the depth. As might be expected from the nature of this relationship, standing waves are obtained in the working section of a free-surface tunnel when operation is near $\mathbf{F}_y = 1$.

Any flow velocity might be matched by the celerity of a wave or surge of very long wave length and large amplitude. Although continuous operation provides sufficient time for waves to grow, their maximum amplitude and celerity can be controlled by limiting their length. The maximum wave length will not greatly exceed the distance between a station near the nozzle exit and the one near the diffuser entrance when the same depth of flow is maintained at these two stations. This wave of approximately the length of the working section will have a celerity that depends on the amplitude to which it grows; but since there is a limit to the wave steepness that can be maintained, height and celerity will be limited.

When the free-surface working channel is long enough to allow growth of a wave that is long compared to the channel depth, the wave celerity, even at low amplitude, will approach $\sqrt{gy}$. It will then, at its highest amplitude, have a celerity greater than $\sqrt{gy}$ and consequently require a channel Froude number

$$\mathbf{F}_y = \frac{V}{\sqrt{gy}} > 1$$

to sweep the working section clear of waves. After going to this higher velocity and sweeping the wave of high amplitude out of the working section, the velocity could then be reduced until the Froude number is only very slightly greater than one without subsequent formation of the high wave. Just how much the velocity can be lowered will depend on the magnitude of the disturbances present; at $\mathbf{F}_y \gtrless 1$, disturbances of small magnitude cause growth of a wave. A mechanism for growth is available since these disturbances produce waves of small but finite amplitude that are not effectively limited in length by the downstream control station. Because of their longer length, these waves have a celerity slightly in excess of the approaching flow and contribute to the growth of the wave of shorter length.

By using a shorter working section, the principal gravity wave might be limited to a length having a celerity considerably lower than $\sqrt{gy}$. With sufficient reduction in the distance between control stations, the wave will reach its maximum height at a channel Froude number less than one. Further increase in tunnel velocity will then reduce the wave amplitude to a very small value before a Froude number of one is reached. The amount below a Froude number of one at which satisfactory operation can be maintained depends on the length of the working section and the magnitude of the disturbances present. Operation at channel Froude numbers less than one is best accomplished when the length of the working section is as short as permissible without interference with the wave pattern produced by the model.

Observations have shown that the Free-Surface Water Tunnel at the Hydrodynamics Laboratory will maintain the wave shown in Fig. 1 at $\mathbf{F}_y = 1.008$ when there is about 9 ft of open channel between two stations where the depth is controlled at 1.74 ft. At $\mathbf{F}_y = 1.014$ the channel is swept clear of waves as shown in Fig. 2. The Froude number can then be reduced to 1.001 without forming the high wave. With the working section length shortened to 7 ft, the highest wave is obtained at $\mathbf{F}_y \eqsim 0.86$ and the height is reduced to a very small value at $\mathbf{F}_y \eqsim 0.96$. The waves are smaller in amplitude when the reduced channel length is used. Further analysis of the action of gravity waves for two channel lengths is given in Appendix I.

Standing waves are not eliminated when the stream velocity is reduced below the minimum celerity of a single wave having a length equal to the distance between the control stations. Under such conditions, a wave of finite amplitude will form in a shorter length so that its celerity will again equal the velocity of the approaching flow. It appears that there will be some type of wave disturbance with an effective length and amplitude that produces a celerity equal to any flow velocity lower than that required to sweep the longest wave out of the working section.

On lowering the velocity through the range that produces waves in a test channel, satisfactory operation is again obtained only when the Froude number is low enough for the resulting waves to be so short and so small in amplitude that they do not materially alter the wave pattern produced by the model under test. The range of Froude numbers where operation is unsatisfactory might be reduced by making the downstream control station in some form that provides an end condition that prevents the growth of waves in the working section. Since the exact nature of such an end condition is not known, further

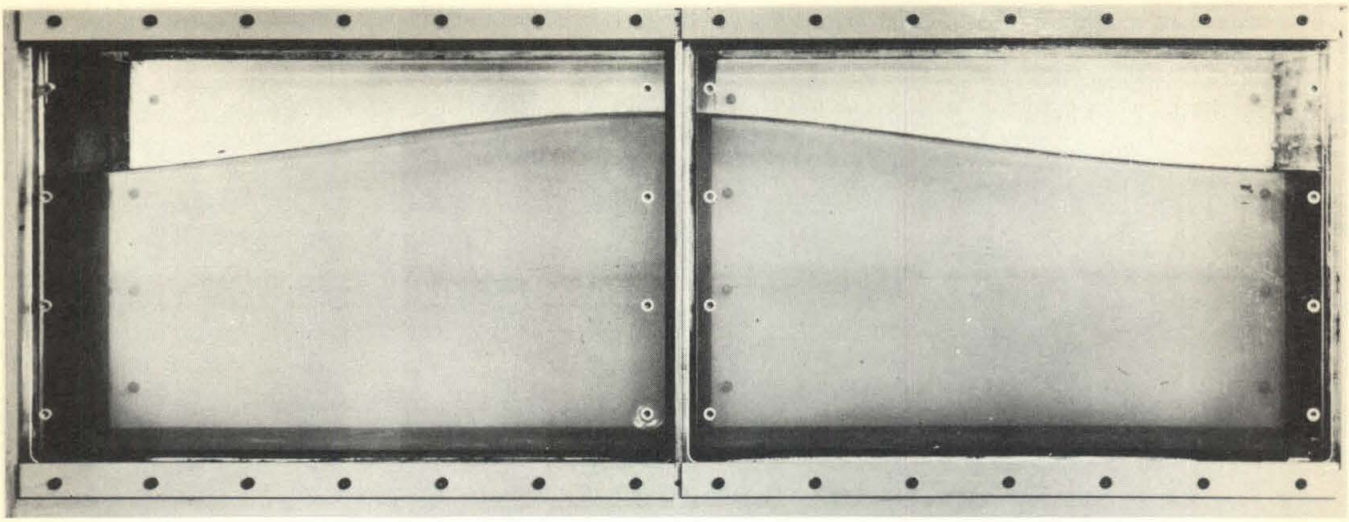

Fig. 1—A Single Standing Wave in the Free-Surface Water Tunnel at $\mathbf{F}_y = 1.008$

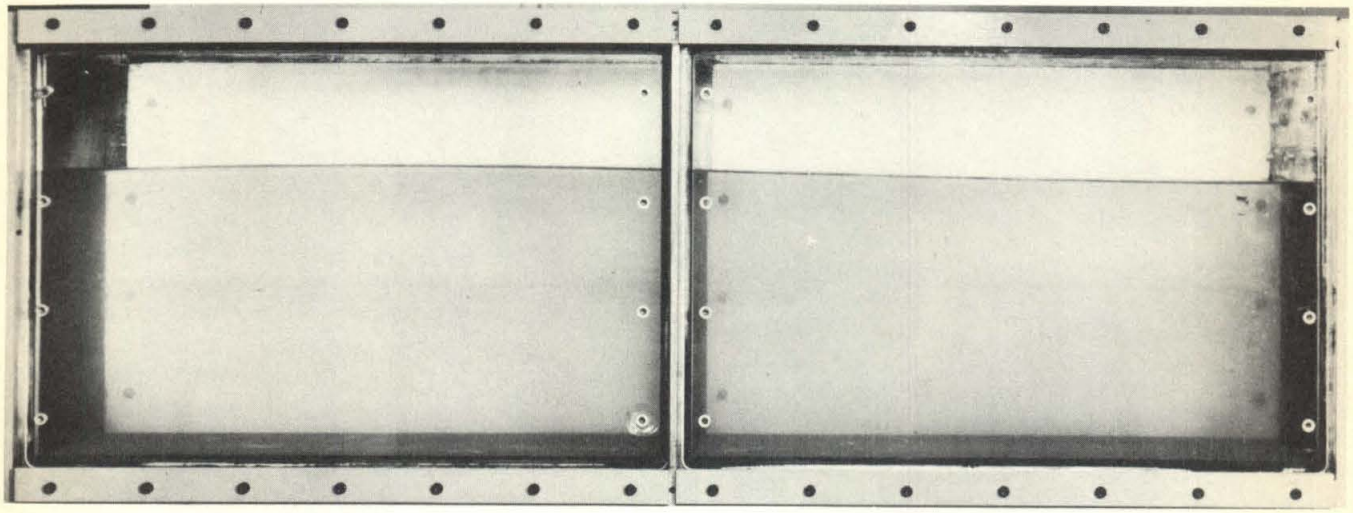

Fig. 2—The Principal Gravity Wave is Swept Downstream and Out of the Working Section at $\mathbf{F}_y = 1.014$

investigation is required before limitations due to wave difficulties can be established.

Relation of Model Froude Number to Channel Froude Number

Since the model Froude number is the similitude parameter for tests in a free-surface water tunnel, its relation to the channel Froude number should be determined. From (2) we have

$$V = \mathbf{F}\sqrt{gl},$$

and since this velocity is the same as that which determines the channel Froude number, we have from (3)

$$\mathbf{F}_y = \frac{\mathbf{F}\sqrt{gl}}{\sqrt{gy}} = \mathbf{F}\sqrt{\frac{l}{y}}$$

which gives the relation

$$\frac{\mathbf{F}_y}{\mathbf{F}} = \sqrt{\frac{l}{y}}\,. \tag{5}$$

This relation is of considerable importance when we consider practical limitations on the ratio l/y and how this affects the required channel Froude number. Cases of particular interest

are those which, with normal l/y values, lead to a channel Froude number that is very high, very low, or in the range that is not permissible because of standing-wave difficulties. In order to consider further the relation between test requirements and tunnel design, the relations presented in a chart for dynamic similitude should be examined.

The Similitude Chart

The flow patterns around a model and prototype cannot be geometrically similar unless they are characterized by the same ratio of unit inertial to unit gravitational forces, that is, by the same Froude number

$$\mathbf{F}_m = \frac{V_m}{\sqrt{gl_m}} = \mathbf{F}_p = \frac{V_p}{\sqrt{gl_p}} \qquad (6)$$

where the symbols are as defined for (2) with the subscripts m and p denoting model and prototype, respectively. Although Froude-number similitude is of primary importance when the flow pattern involves gravity waves at an interface, it is accomplished with a resulting dissimilitude of viscous and surface-tension effects when both model and prototype operate in contact with the same fluid. To evaluate this dissimilarity between model and prototype, we determine the value of their criteria of similitude: Reynolds number

$$\mathbf{R} = \frac{Vl}{\nu}, \qquad (7)$$

where ν is the kinematic viscosity, for viscous effects and Weber number

$$\mathbf{W} = \frac{V}{\sqrt{\sigma/\rho l}}, \qquad (8)$$

where σ is the surface tension and ρ the density of the fluid, for surface-tension effects.

As an aid to planning and analyzing tests in the Free-Surface Water Tunnel at the Hydrodynamics Laboratory, the dynamic-similitude chart shown in Fig. 3 has been prepared. The evaluation of the slopes and positions of the lines is presented in Appendix II. With Froude number as abscissa and model or prototype length as ordinate, the chart presents a network of sloping lines of constant velocity, Reynolds number, and Weber number; constant Froude number is represented by the vertical lines and constant length by the horizontal. Operating conditions for a model or prototype are represented by a point on the chart.

The operating point of a prototype of known length and velocity can be located on the similitude chart by finding the prototype velocity on the velocity scale and following, from this point, a line of constant velocity until it intersects the line representing the prototype length. From the operating point represented by this intersection, lines parallel to those of constant Reynolds and Weber numbers can be followed until they intersect the appropriate scales where the values of these numbers can be read. By following a vertical line from the operating point to the abscissa scale, the Froude number can be read; this vertical line of constant Froude number is then the locus of all possible model-operating points that maintain inertial-to-gravitational similitude. From the intersection of this vertical line with the horizontal line representing the desired model size, that is, from the model-operating point, lines of constant velocity, Reynolds number, and Weber number can be followed to the appropriate scales to find the model velocity required for gravitational similitude and the resulting values of Reynolds and Weber numbers that differ from those for the prototype.

It might be noted further that the vertical distance between the model- and prototype-operating points, when laid off along any of the logarithmic scales, starting at 1.0, will end at the value of the ratio of the prototype to model length. The reciprocal of this value, the model-to-prototype scale $\lambda_{mp} = l_m/l_p$, is obtained in a similar manner by measuring backwards along the logarithmic scales. It is obvious from the slopes of the lines on the similitude chart that a wide spacing between model- and prototype-operating points results in a large dissimilitude of Reynolds and Weber numbers. By using the largest model permissible without excess boundary interference, this dissimilitude is minimized.

The operating range of a free-surface water tunnel (or towing tank) can be represented by an area in the lower-left corner of the similitude chart. For a tunnel with a fixed working section, this operating range is bounded at the top by a line representing the maximum permissible model size as limited by boundary interference; the boundary at the right is determined by the line representing the maximum tunnel velocity. An example of what might be the operating range of a tunnel is represented in Fig. 4 by the area below and to the left of the line ABC. A model test, in which the ratio of unit inertial to gravitational forces is the same as for the prototype, could be made for any prototype that has an operating point directly above this tunnel-operation area. Not all points in the tunnel-operating area, however, are equally amenable for test purposes.

To minimize Reynolds and Weber number dissimilitude, tests should be conducted at operating points near the line ABC where the model is as large as permissible for the Froude number involved. There will be a range of model Froude numbers, however, that can be obtained only by reducing the model size below that represented by line AB. This is necessary in order to avoid the channel Froude numbers that result in wave difficulties. An example of a likely forbidden area of operation is shaded in Fig. 4. This example is based on the assumptions that, (1) in a working channel that is 3 ft deep, 6 ft is the limit on model length in order to avoid boundary errors, (2) $\mathbf{F}_y = 1.1$ is the minimum usable channel Froude number for which the primary channel wave is swept out of the working section, and (3) $\mathbf{F}_y = 0.5$ is the maximum channel Froude number for which small surface waves can be

tolerated.* It is seen to be necessary for complete Froude-number coverage in this range,** to employ models as small as about 1.1 ft. in length; the small model length obviously results in reduced values of Reynolds and Weber numbers. It is difficult to avoid a gap in the usable range of $\mathbf{F}_m$ when the shaded zone is wide.

Reduction of Reynolds- and Weber-Number Dissimilitude

Further examination of the tunnel-operation area on the similitude chart shows that the highest Froude numbers were obtained by reducing the model size after the maximum tunnel velocity was reached. This reduction in the model size not only results in diminished values of Reynolds and Weber numbers, but is ineffective in achieving a large increase in Froude number without employing models that are absurdly small compared with dimensions of the working channel. The lowest Froude numbers are achieved at quite low velocities and consequently with extremely small utilization of the available power. Since only the tests at Froude numbers that allow operation near point B on the similitude chart fully utilize the potentialities of the tunnel, a method of changing this point to other Froude numbers should be considered.

The higher Froude numbers could be obtained with less reduction in model size, and consequently with less Reynolds- and Weber-number dissimilitude, if the channel cross section and the model were reduced proportionately since it would then be possible to get a higher velocity with the available power. Conversely, the low-Froude-number tests would have less dissimilarity of Reynolds and Weber numbers if the available power were used to pump water through a larger channel containing a proportionately larger model. With the same basic tunnel outside the working-section zone (and this basic tunnel may account for the major portion of the investment), minimum discrepancy of Reynolds and Weber numbers is maintained when the working section is varied in such a way that all tests can be made at maximum power with a model that is the maximum size permitted by boundary effects.

The range of operation of a tunnel with adjustable channel dimensions is represented on the similitude chart by the area bounded by the locus of the changing position of point B as the channel size is varied. The position of this boundary line as well as the nature of any limitations on the variation of working-section dimensions should be considered.

The Operating Range of a Tunnel with a Variable Working Section

The operating range of a tunnel with a variable working section can be indicated on the similitude chart for comparison with the boundary ABC (Fig. 4) for a fixed channel. Conditions at any point on the operating boundary can be made similar to those at point B by keeping the ratio of the model size to the channel size as high as is permitted by wall effects and varying the two together in order to utilize all the available power at any Froude number desired. Limits can be established for the slope of such a boundary line. Consider the case of a tunnel in which, throughout the range of variation of working-section dimensions, the head losses are a constant per cent of $V^2/2g$ where V is the velocity in the variable working section. Such a condition might be approached when the return circuit is large enough that practically all the losses occur in the working section and diffuser. Then, since power $\propto QV^2$ where Q is the volume rate of flow, continuous utilization of the maximum available power* to overcome these losses would result in a constant value for QV^2. Since $Q \propto l^2V$ and since, from (2), we have $V \propto \mathbf{F}l^{1/2}$, these conditions can be represented on the similitude chart by a line with the slope produced when $\mathbf{F}^3l^{7/2}$ is held constant. The line MN in Fig. 5 is drawn with this slope.** Consider also the case of a tunnel with a very small return circuit in which practically all the losses occur. Constant power will then result in constant Q. Since again we have $Q \propto l^2V$ and $V \propto \mathbf{F}l^{1/2}$, these conditions are represented by the line OP where $\mathbf{F}l^{5/2}$ is held constant. It might be expected that the real operating boundary would approach reasonably close to the slope of case 1 at the higher Froude numbers where the working section is smallest and the velocity high compared with the return circuit. If it should be estimated that case 2 is not likely to be approached closely even for the largest channel, these rough assumptions are sufficient to fix the position of the real operating boundary as close as necessary for the present discussion.

An estimated likely form of the boundary of the operating area of a variable-channel tunnel has been drawn as line DBE in Fig 5. Point B is the same as that used in Fig. 4 to illustrate the fixed working section. The operating range of two tunnels with the same return circuit and pumping equipment, one tunnel having a fixed and the other a variable working section, are consequently compared by the difference in the position of lines ABC and DBE. It is obvious that the tunnel with a variable channel permits tests to be made with larger models and higher velocities for all Froude numbers except the one obtained when operating at point B.

The operating area that cannot be used because of standing wave difficulties has again been indicated by a shaded region in Fig. 5. This was based on the same assumptions used for obtaining the corresponding area in Fig. 4, that is, channel Froude numbers from 0.5 to 1.1 are excluded and model lengths up to twice the channel depth are allowed. In the

* These assumptions should be the subject of further analytical and experimental investigations. Recognition of the existence of the limitations is sufficient to allow formulation of the basic hydrodynamic principles of the free-surface water tunnel.

** Note that $\mathbf{F}_m = 0.8$ can be obtained with either $l_m = 6$, $V = 11$, $\mathbf{F}_y = 1.12$ or $l_m = 1.1$, $V = 4.8$, $\mathbf{F}_y = 0.482$.

* Constant efficiency of the motor and pump is assumed. The problem of maintaining high efficiency under varying head requirements is discussed later.

** A greater slope might possibly be obtained if, in the range where nozzle contractions are high enough for negligible losses in the return circuit, the lowered turbulence level due to an increase in contraction ratio results in a lower percentage of regain of velocity head by the diffuser.

DYNAMIC SIMILITUDE NEAR AN AIR-WATER INTERFACE

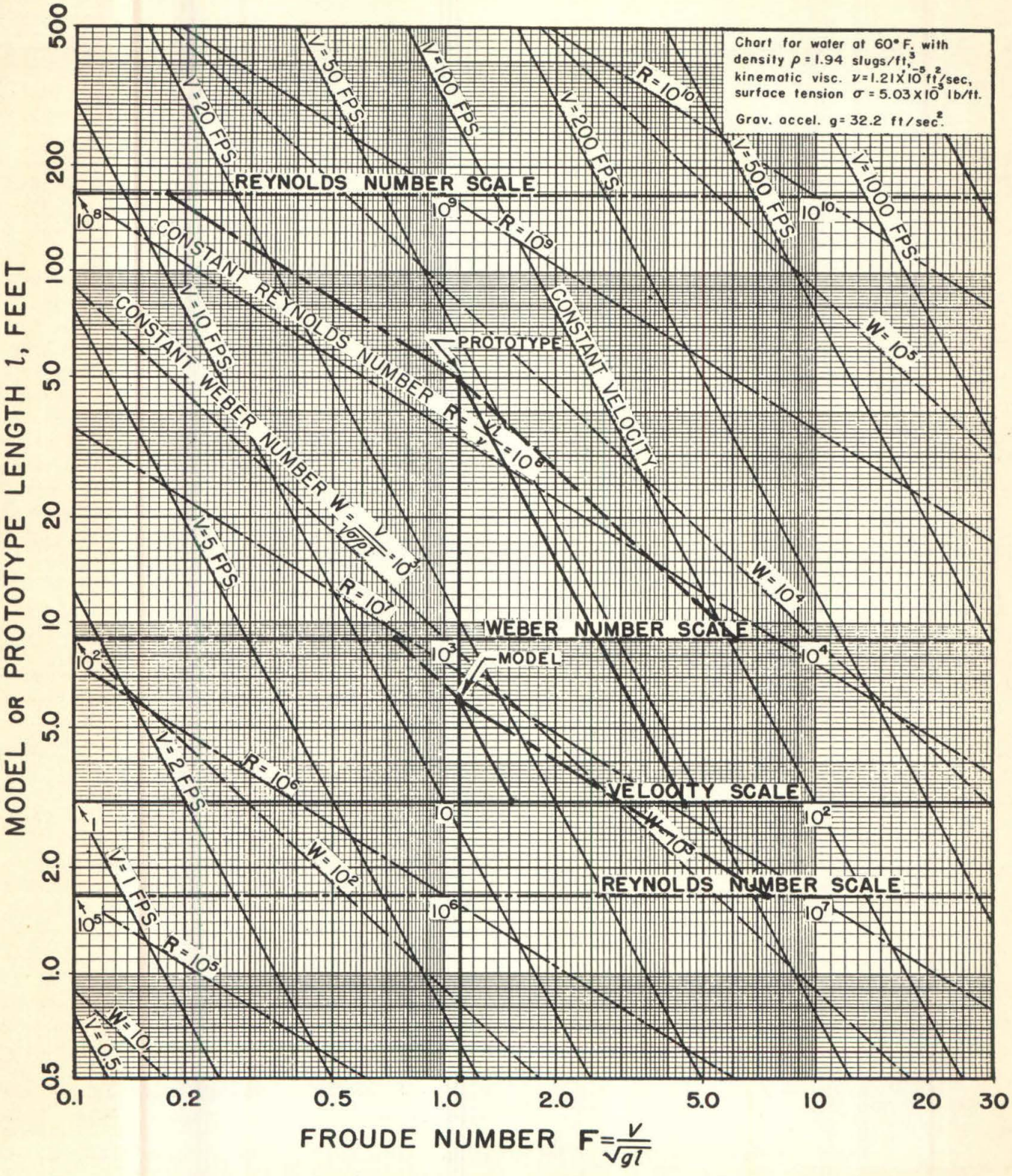

Fig. 3—The Operating Conditions for Froude-Number Similarity Between a Model and a Prototype are Shown on the Similitude Chart.

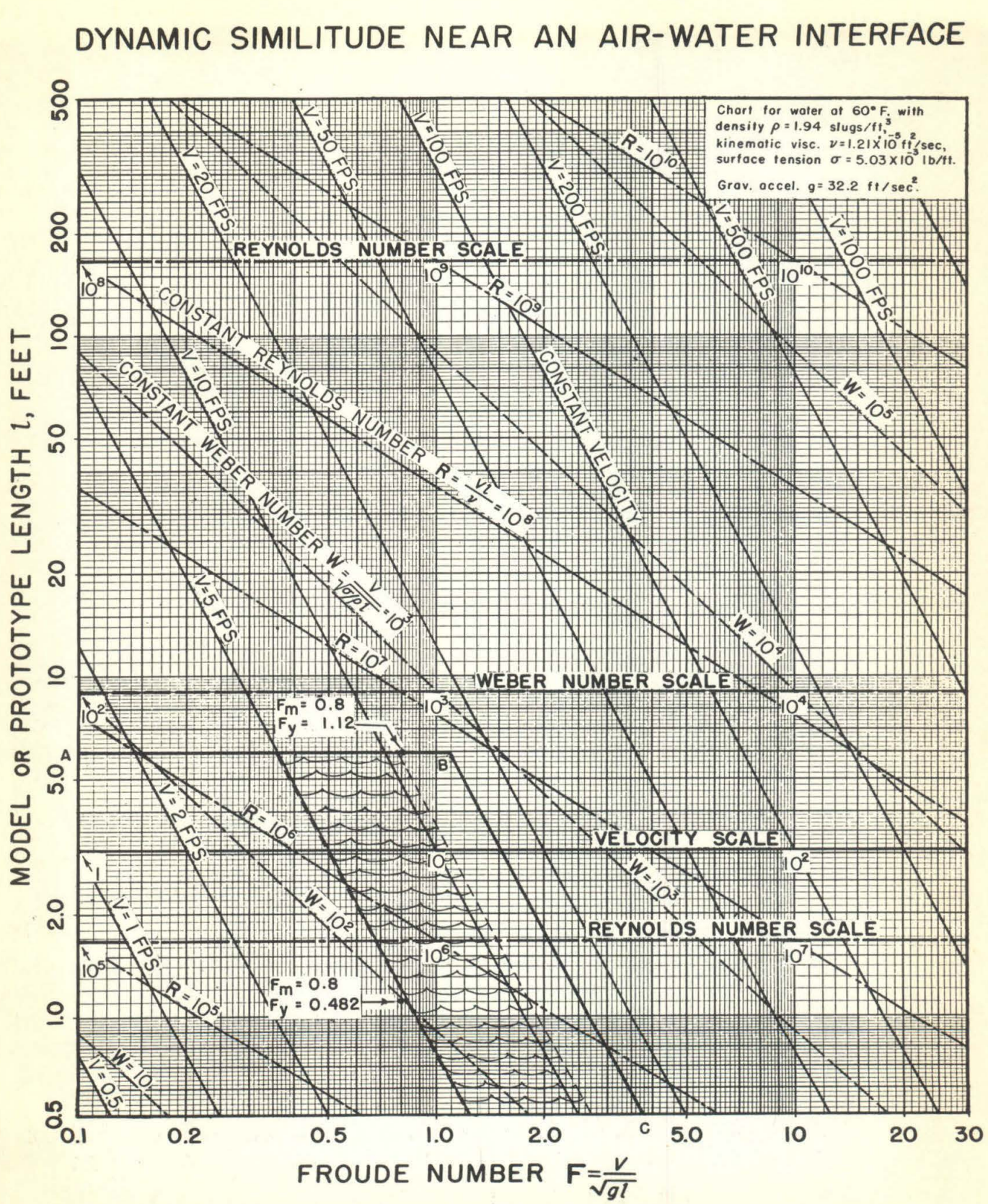

Fig. 4—The Use of the Similitude Chart for Indicating the Operating Range of a Free-Surface Water Tunnel with Fixed Working-Section Dimensions.

DYNAMIC SIMILITUDE NEAR AN AIR-WATER INTERFACE

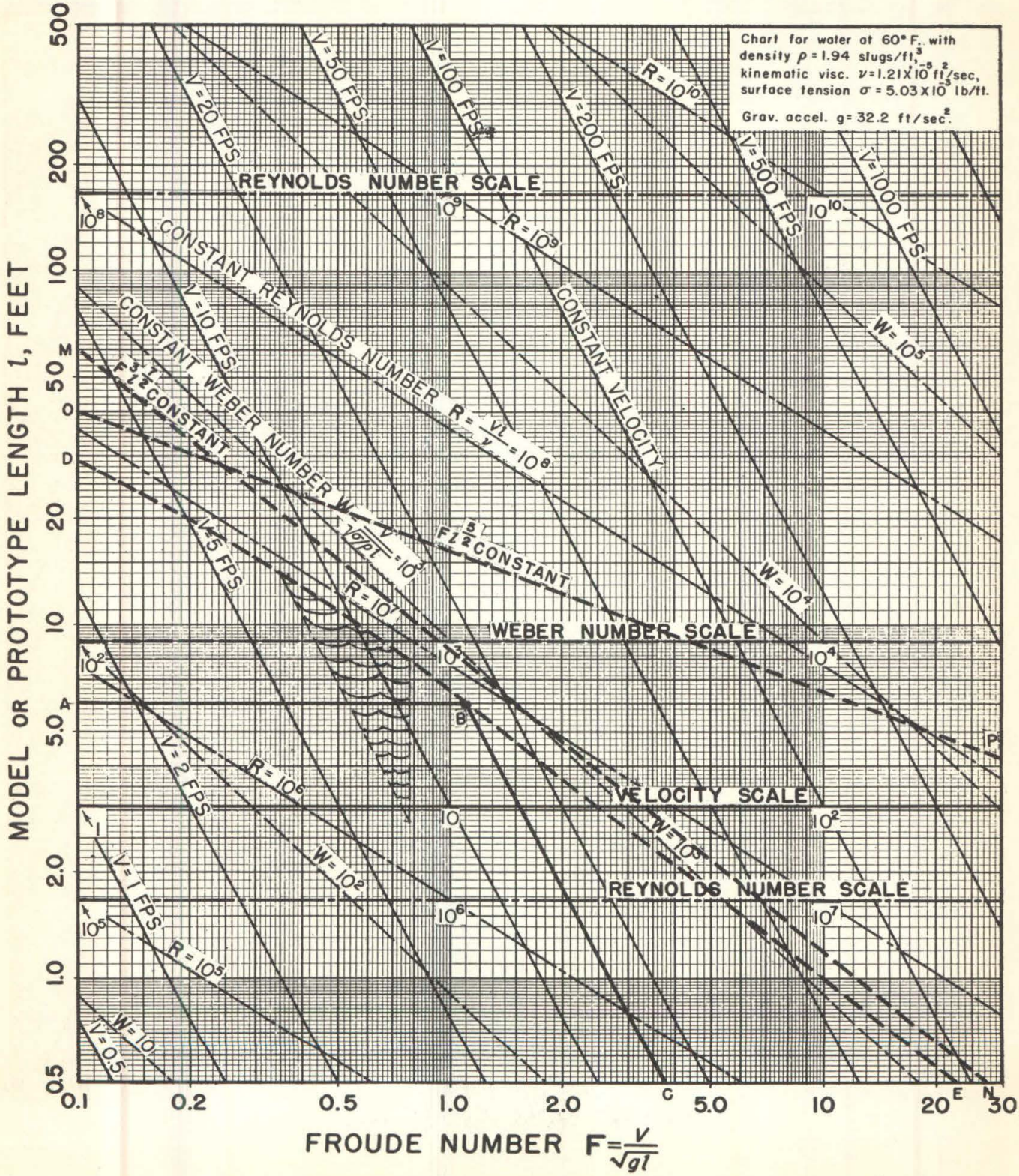

Fig. 5—The Operating Range of a Free-Surface Water Tunnel with a Variable Working Section

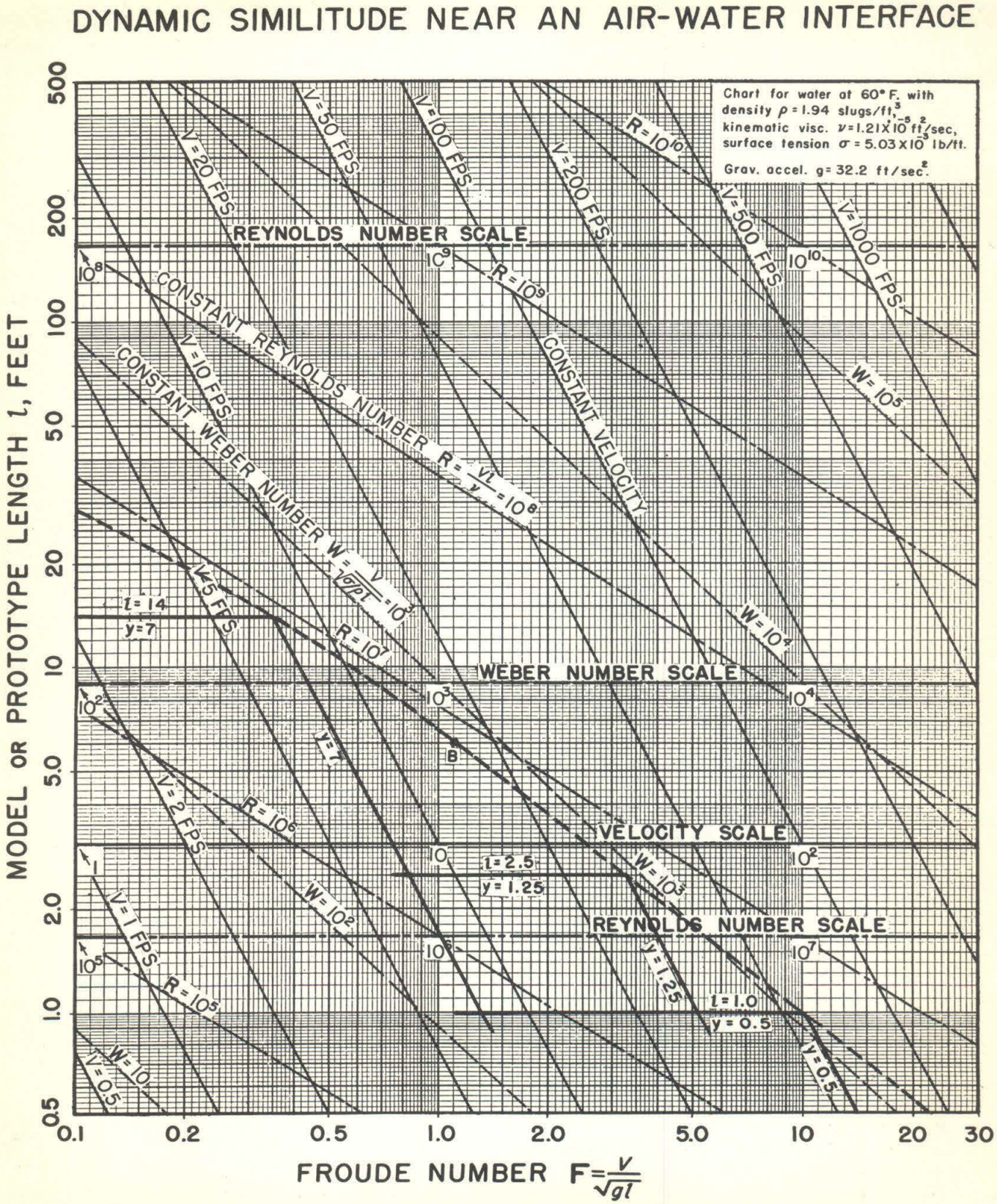

Fig. 6—The Operating Range of a Free-Surface Water Tunnel having Three Channel Sizes

tunnel with variable channel dimensions the shaded area is greatly reduced.

Determination of Tunnel Size and Power

Before considering the choice of size steps that might be used in carrying out the principle of the variable working channel, the method of determining the position of the boundary of the operating range, and consequently the tunnel size and power, might be investigated further. The Froude-number range of the craft to be modeled would naturally be considered in determining the requirements of a new facility for test and research. It should be borne in mind, however, that basic investigations involving inertial-to-gravitational similitude are often incomplete unless the ratio of the inertial to the gravitational forces is varied throughout the range where significant differences in hydrodynamic effects are detectable.

In order to determine the Reynolds- and Weber-number dissimilitude at various Froude-number ranges, the upper boundary of anticipated prototype-operating points might be drawn on the similitude chart and compared with a proposed tunnel-operation boundary. This dissimilitude is obviously reduced throughout the range by raising the tunnel-operation boundary. Raising the entire boundary, however, involves an increase in both size and power with a consequent rapid increase in cost. First consideration should therefore be directed toward the development of a tunnel having an operating boundary above any critical zone where there is an irregular change in Reynolds- or Weber-number effect. Since the operating boundary for a variable-channel tunnel has about the same slope as a constant-Reynolds-number line, and since Weber-number effects may be more critical at high Froude numbers where flow in thin sheets and spray from planing surfaces are involved, the variable working section will be found effective in producing an operating boundary above these irregularities in the Reynolds- and Weber-number laws and in minimizing the remaining dissimilitude effects throughout the desired Froude-number range.

Whether an operating-boundary level is attained with a return circuit of large size and minimum power or with a smaller circuit by means of higher power, may have considerable influence on the required total initial investment and subsequent operating costs. Such manipulation of tunnel proportions will influence the slope of the operating boundary within the limits set by lines MN and OP in Fig. 5. It is important, therefore, to consider the nature of this influence and to determine limitations on such manipulation.

An operating boundary, such as DBE, Fig. 5, is shifted to the right by increasing the power. By such a change in the position of the operating boundary, the velocity attainable for each model size is multiplied by some factor; an increase in power by the cube of this factor is required to produce the higher velocity. This tunnel with higher power, but with no change in return-circuit dimensions, could then have a still further increase in channel size for the low Froude numbers. On the similitude chart, this increase in channel and model size is represented by a continuation of the operating-boundary line. The part of the operating-boundary line that is added, however, will approach closer to the slope OP since this is the limiting slope for a power level so very high that the desired Froude numbers can be attained in channels that are so large compared to the return circuit that working-section losses are negligible.

Possibly the most important limitation on the use of a high power level would be due to loss of adequate control of turbulence level and velocity distribution in the working channel. This might occur when the cross-sectional area of the working channel approaches or becomes larger than the return circuit. This may, however, be found to have sufficient influence on the cost to warrant an investigation determining the minimum nozzle-contraction ratio permissible for the largest working channel to be used. Consideration should be given to the use of some space and power for honeycombs and damping screens since, if turbulence and velocity-distribution conditions determine the permissible nozzle ratio, this would permit a smaller return circuit. Very little loss would occur in such a flow-control space when the smaller working channels are in use. It seems probable that the cross-sectional area of the largest channel might be allowed to be larger compared to the return circuit than in conventional tunnels, because the low contraction ratio would be obtained only for the low Froude numbers.* Investigation of the possibility of a reduction in total cost by this expedient seems particularly intriguing when it is considered that some tests at low Froude numbers have utilized artificially-generated turbulence ahead of the model.

If the size of the return circuit of a tunnel is increased, the operating boundary on the chart is raised where its slope departs from the slope MN, that is, at the left end of the operating boundary. Its position is not changed at the right end if the slope there is essentially the same as MN. Once the return circuit becomes large in comparison with the working channel, further increase in return-circuit dimensions does not add materially to the operating area on the similitude chart. Such an increase in dimensions becomes costly and finally ineffective compared with an increase in power. The minimum return circuit dimensions allowable when turbulence is considered will determine the optimum proportions.**

The operating boundary established by the methods discussed so far has been based on a continuously variable channel which is impractical. Such a boundary indicates the possibilities and limitations of the basic circuit and, when used in

* In a closed-circuit tunnel that does not have a free surface, the principles that lead to the consideration of a variable working section do not apply. If, however, the similitude chart were used to show operating characteristics obtainable for various working section sizes (ignoring Froude and Weber number lines), the nozzle contraction ratios usually employed may lead to an operating-boundary slope approaching MN. Comparing the slope MN with a constant Reynolds number line, it is apparent that higher Reynolds numbers result from the use of smaller contraction ratios and larger working sections. If Reynolds number is used as the design criterion for such a tunnel and if the difficulty of using small models is also considered, it appears that the contraction ratio should be only high enough for adequate control of turbulence and velocity distribution.

** If turbulence and velocity distribution should be found satisfactory with a small return circuit compared with even the smallest working section, as is unlikely when high Froude numbers are to be obtained, optimum proportions would be based on relative cost of attaining the desired operating boundary by means of high power or by use of large return-circuit dimensions.

conjunction with the indicated area of operation where waves cause difficulty, it serves as a guide to the selection of size steps for the working section.

Choice of Size Steps for the Working Channel

On the similitude chart, the operating boundary for a tunnel having a working channel that is changeable by finite size steps will be a zig-zag line having alternate segments representing constant model length and constant velocity. The lines will be located below the curved line, such as DBE, Fig. 5, representing the operating boundary of a continuously varying channel; the intersections representing maximum velocity and model length for each channel size, however, will be on this curved line. A number of small operating areas bounded by a line of constant velocity, a line of constant model length, and a segment of line DBE are not available for tunnel operation when the channel size is changed by steps. The most important principle to be observed in the choice of channel size steps is to select two sizes so that the resulting unavailable operating area includes the shaded area (Fig. 5) that cannot be used because of standing-wave difficulties.

With two channel sizes selected to avoid standing-wave difficulties, the lowest desired Froude numbers might be obtained by reduction of velocity while using the largest permissible model in the larger channel and the highest Froude numbers obtained by reduction of model size while using maximum velocity in the smaller channel. As previously pointed out, however, large reduction in velocity or model size may result in a failure to utilize, at these extreme limits of the Froude-number range, the full potentialities of the major part of the investment in the entire facility. A wide Froude-number range may consequently warrant the use of additional channel sizes.

The example that has been followed through the continuously variable operating boundary DBE in Fig. 5 is presented in Fig. 6 as a tunnel with three channel sizes covering model Froude numbers from 0.1 to 14. The boundary lines represent operation as follows: With a 14-ft model in a channel that is 7 ft deep, model Froude numbers from 0.1 to 0.35 are obtained by varying the velocity from about 2 fps to full-power operation at 7.4 fps. Operation is maintained at full power with the largest channel while the model length is reduced from 14 ft to 2.5 ft for Froude numbers from 0.35 to 0.82. The 2.5-ft model can be checked at $\mathbf{F} = 0.82$ in the next smaller channel (1.25 ft deep) to provide overlapping tests in the two channels—the larger operating below the velocities producing wave disturbances and the smaller operating above the critical velocity range. The 2.5-ft model is then used as the velocity in the stream having a depth of 1.25 ft is increased to full power again at 29.6 fps where the Froude number is 3.3. Full power and a decrease in model length to 1 ft then takes the Froude number to 5.2 where the test can also be made in the smallest channel which is 6 in. deep. This channel can then be used with the 1-ft model to $\mathbf{F} = 10$ at 56 fps where a reduction in model length to 6 in. gives a model Froude number of 14.

It may be noted that the channel sizes selected did not include the original example of Fig. 4 since it would be only of limited usefulness in filling out a small area to the right of the shaded zone of Fig. 5. Tests in this area would not include a test point that could be checked in the next larger channel, as is the case for the channel that takes models up to 2.5 ft long. For these reasons it is doubtful that a channel having its operating point for maximum velocity and model length to the right of the shaded area is warranted. The channel size that is least desirable is one having its maximum velocity at the high end of the range where waves cause difficulty, that is, at a channel Froude number of about 1.0.

The examples selected to illustrate the synthesis of a tunnel design are based on a number of assumptions that, during an actual tunnel-development project, should be arrived at by further analysis and experimental investigation. Possibly the most important factor in determining the tunnel proportions is the decision regarding allowable turbulence in the working channel since this will set limits on the nozzle contraction and determine the requirements for grids and screens in the approaching flow. Having established the size of the upstream end of the nozzle, a layout of the return circuit can be made. From this preliminary layout and loss estimates, the pump and power requirements can be determined and a more accurate boundary can be established for the operating zone of the tunnel with a variable working channel. Another major investigation should be directed toward the determination and reduction of the range of channel Froude numbers that cause difficulty because standing waves are formed in the working section. This is of primary importance in the selection of size steps for the working channel—possibly even to successful operation at model Froude numbers just below the lowest obtainable with waves swept out of the working section. The assumptions made here, however, are believed to be adequate for illustrating a method of arriving at the basic design of a closed-circuit tunnel.

Design of Tunnel Components

Most of the available literature that is useful to the designer of a closed-circuit tunnel deals with the performance of tunnel components. It is not intended that this discussion of the hydrodynamics of the basic circuit should include a detailed consideration of the various tunnel components but some of those affected by the unusual features suggested are noted.

In order to avoid excess corner disturbances in a channel with a rectangular cross section, the approaching flow should come through a series of two-dimensional nozzles designed to receive and discharge parallel flow. Alternate vertical and lateral contractions can then be bolted together to terminate at the channel cross sections desired. Although the basic size steps would be made on the basis of channel depth, the depth-to-width ratio could be made either about 1 to 1 for testing bodies that operate with shallow submergence or about 1 to 2 for testing surface craft. This change in depth-to-width ratio could be accomplished by either using or omitting a final nozzle section with lateral contraction. The termination with

vertical contraction for testing surface craft provides better control of the velocity profile near the surface since it squeezes down the thickness of the boundary layer that was developed in the preceding section having a flat roof. For typical operating conditions, the pressure at the top of the vertically-contracting nozzles should be calculated to determine the requirements for keeping the nozzle filled and to determine the cavitation characteristics.

The transition from the free-surface stream to an enclosed diffuser is readily made by skimming off a thin surface layer at the diffuser entrance and returning this water through an auxiliary circuit.* The diffuser sections must also have a two-dimensional flare in order to avoid difficulties in the corners of the rectangular conduit.

An air separator in the low-velocity stream following the diffuser necessarily has a free surface where bubbles are collected. Again it is necessary to have a transition to a closed conduit leading to the suction side of the circulating pump. It may not be necessary in this case, however, to skim off a surface layer at the transition since the velocity is low and the active stream can be submerged below a pool to prevent entrainment of air. It is necessary to provide a pressure differential between this low-velocity air-separator section and the working section in order to realize the velocity-head regain that the diffuser is capable of delivering to the suction side of the pump. Furthermore, this pressure differential should be regulated since it controls the depth at a station at the downstream end of the working channel.

The total length of nozzle, working section, and diffuser can be made the same for the various size steps in the working section, since it is the smaller (and shorter) channels that require a long diffuser. Adjustments can be made by making the downstream diffuser section, where required, in the form of a vaned diffuser of short length.

The losses in a tunnel with a single fixed working section can usually be calculated with sufficient accuracy to permit a fixed-pitch propeller pump to be specified. The losses in this case remain sufficiently constant to keep the operation near the peak of pump efficiency. In a tunnel with a variable channel, however, the resistance and head requirements will vary so much that good efficiency can be maintained only by varying the pump characteristics. This might be accomplished by varying the pitch of the propeller,[2] varying the angle of the approach and discharge vanes, or by some combination of these methods. The selection of cavitation characteristics of the pump, as is usual, will be made on the basis of static submergence and the minimum pressure to which the tunnel might be exhausted for the purpose of obtaining low cavitation parameters in the working section.

* This is described in more detail in reference 1.

[2] "Comparative Characteristics of Fixed- and Adjustable-Blade Axial-Flow Pumps," by J. D. Scoville, Trans. ASME, Vol. 64, No. 6, 1942, pp. 599-606.

Operation of the Free-Surface Water Tunnel at the Hydrodynamics Laboratory

A drawing of the Free-Surface Water Tunnel at the Hydrodynamics Laboratory of the California Institute of Technology is shown in Fig. 7. The cross section of the working section was made approximately square since it was intended primarily for testing models of craft that operate at shallow submergence. Using a model length up to 2.5 ft in the working channel that is 1.74 ft deep would result in an operating area approximately as shown in Fig. 6 for the intermediate size of working channel.

No difficulty is encountered in going through the critical velocity of this tunnel and sweeping the standing waves out of the working section. The flat surface profile is then controlled primarily by the nozzle dimensions and the operation is satisfactory, as shown in Fig. 2, at channel Froude numbers above 1.02. The work with this tunnel at the Hydrodynamics Laboratory has been entirely at these higher velocities where the principal gravity wave is eliminated. As discussed in Appendix I, however, brief operation for the purpose of noting the wave action at lower velocities seems to indicate that careful consideration of the characteristics of waves of finite amplitude in channels of finite depth and length may lead to extended use at low Froude numbers. There should be more experience in actual operation at Froude numbers below 1.0 at the David W. Taylor Model Basin.[3]

In order to conserve space, the diffuser in the Free-Surface Water Tunnel at the Hydrodynamics Laboratory was made short by using closely spaced turning vanes. Since this has resulted in low efficiency (about 35% of the working-section velocity head is regained), it is recommended that room be allowed for a two-dimensional diffuser of conservative flare with few or no internal dividing plates so that a greater portion of the velocity head can be applied to the suction side of the pump. Closely spaced vanes might be used, however, in the downstream section of the diffuser where the remaining velocity head is small in comparison with the losses in other parts of the circuit.

Although a large quantity of air, even in the form of small bubbles, can be extracted by the air separator, a few bubbles circulate through the working section at the highest velocities. The difficulty has not warranted a delay in other programs to find the cause and cure; it is believed, however, that this circulation of air might be avoided if the conduit leading from the air separator to the pump had a roof that extended upstream into a pool above the active stream. The roof over the air space above this pool should not slope downwards to meet the conduit mouth as this might cause entrainment of air.

Summary of the Hydrodynamic Characteristics of a Free-Surface Water Tunnel

A closed-circuit tunnel having an air-water interface at the

[3] "The Characteristics and Utilization of the David W. Taylor Model Basin Circulating Water Channel," C. A. Lee, Proc. Third Hydraulic Conference, University of Iowa, 1946, pp. 277-297.

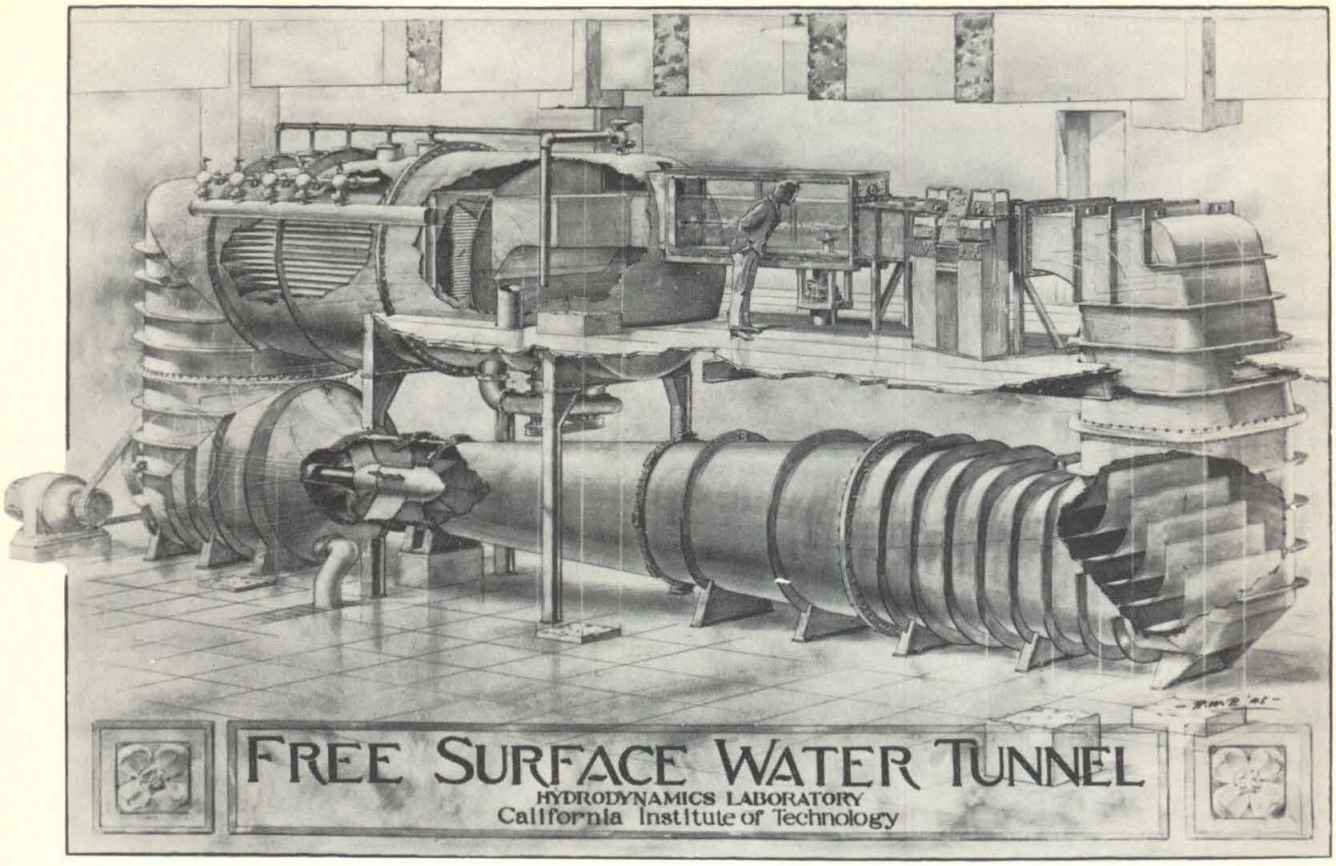

Fig. 7—The Free-Surface Water Tunnel at the Hydrodynamics Laboratory of the California Institute of Technology

working section can be used to establish relative motion between the water and a test object or model. Surface waves are produced by such relative motion when the model is held so that it intersects or is near the interface.

The hydrodynamic forces on a model will be similar to those on a prototype surrounded by a flow pattern of identical geometrical configuration. Obviously this identity requires geometric similarity of model and prototype dimensions as well as position relative to the surface. Furthermore, since the surface-wave contours form part of the boundaries of the flow pattern, it necessarily follows that the waves produced by the model should be similar to those produced by the prototype.

The surface-wave pattern is controlled primarily by the ratio of the unit inertial to the unit gravitational forces. This ratio is given by

$$\frac{\rho V^2/l}{\Delta\gamma}$$

where V is the velocity of the relative motion, ρ is the density of the water, l is a characteristic length, and $\Delta\gamma$ is the difference in the specific weights of water and air. Then, since the specific weight of air is very much smaller than that of water, $\Delta\gamma$ is almost equal to the specific weight γ of water and since γ/ρ is equal to the gravitational acceleration g, dynamic similitude between model and prototype is achieved by having identical values of the Froude number which reduces from the above ratio to

$$\mathbf{F} = \frac{V}{\sqrt{gl}}.$$

A channel Froude number

$$\mathbf{F}_y = \frac{V}{\sqrt{gy}},$$

where y is the depth, determines the configuration of waves that depend on the dimensions of the channel. There will be a range of channel Froude numbers in which these waves will be large enough to interfere with the measurement of the hydrodynamic forces that result from the local wave created by the test body. This range is difficult to avoid since the relation

$$\frac{\mathbf{F}_y}{\mathbf{F}} = \sqrt{\frac{l}{y}}$$

indicates that the model and channel Froude numbers cannot be greatly different without using undesirable model sizes.

Another consequence of Froude-number similitude is a dissimilitude of viscous and surface-tension effects. This is shown on the similitude chart of Fig. 3 as a difference in the slopes of lines of constant Froude number and those of constant Reynolds and Weber number. When the operating range of the tunnel is indicated on the chart (ABC in Fig. 4) it is noted that only at point B is the tunnel being most effectively used. The higher and lower Froude numbers could be obtained with less Reynolds- and Weber-number dissimilitude if the working section were varied in cross section to utilize, at any Froude number, all the available power to pump the water around the largest permissible model as limited only by errors from wall effects. The increased operating range indicated by the boundary DBE in Fig. 5 is obtained even though the remainder of the circuit, which accounts for the major portion of the investment, remains essentially the same. It appears that the most economical return circuit will be one having the smallest cross section that will allow sufficient nozzle contraction to adequately control turbulence and velocity distribution in the working section.

The free-surface tunnel with a variable working section will have less interference from the channel waves that are obtained at low Froude numbers. The comparison is indicated by the smaller shaded area of Fig. 5 compared with that of Fig. 4. In the case of the variable tunnel, however, the shaded area can be included as part of the area that is lost due to the necessary use of finite size steps as indicated by Fig. 6. By proper selection of the working-section sizes used, it is evident that wave difficulties are minimized.

The above analysis of the principles of tunnel design has led to many questions requiring further experimental and analytical investigation. The principal objective was not to answer these questions and make specific recommendations, but rather to formulate a basic design concept that insures recognition of the most significant problems.

— — — —

APPENDIX I

Waves in the Free-Surface Water Tunnel

The Free-Surface Water Tunnel at the Hydrodynamics Laboratory was operated with an open working section of two different lengths while the channel Froude number was varied through the range in which surface waves are produced. Observations on these waves may serve as an indication of what might be expected from similar channels of different depths when operating in the same Froude-number range.

The tunnel was operated with the nozzle lip at an elevation $y = 1.74$ ft above the horizontal channel floor. This same elevation was maintained in a gage glass connected to piezometer openings through the channel floor and side walls at the downstream control station. Depth adjustments at this station could be made by varying the back pressure on an enclosed diffuser which received the flow at a point about 0.5 ft. farther downstream. This adjustment could be maintained even though a considerable amount of water was required to fill out the wave crests. A pool in the air separator that follows the diffuser has a second free surface that can vary in elevation to provide the water needed as the waves grow. If water were not supplied to the working section as the waves grow, they would not reach as great a height but the wave troughs would be lower and the downstream control station could not be always maintained at the normal control level. The distance between the nozzle lip and the downstream control station is 9 ft. Operation with an open-channel length of both 7 and 9 ft was accomplished by either using or omitting a 2-ft extension on the nozzle. With the 9-ft channel (about 5.2 y), the conditions of operation were noted in sequence as follows:

1. $h_1{}^* = 2.61$ ft, $V^* = 7.54$ fps, $\mathbf{F}_y{}^* = 1.008$, $y' = 2.07$ ft (elevation of wave crest). This velocity in the 9-ft open channel was slowly approached to produce the highest wave attainable in the absence of a model or other obstruction.
2. $h_1 = 2.62$, $V = 7.59$, $\mathbf{F}_y = 1.014$, no wave. At this velocity the wave is swept out of the working section.
3. $h_1 = 2.61$, $V = 7.54$, $\mathbf{F}_y = 1.008$, no wave. After sweeping the wave from the channel, operation at $\mathbf{F}_y$ only slightly higher than 1.0 is possible.
4. $h_1 = 2.60$, $V = 7.49$, $\mathbf{F}_y = 1.001$, $y' = 1.80$. There is a slight rise with the crest about 5.5 ft. from the nozzle exit. (At high Froude numbers, the level here is about 1.76 ft.)

* The piezometric head h_1 (measured relative to the channel floor) is for a station at the upstream end of the nozzle. Velocities given above were calculated by applying Bernoulli and continuity equations between the upstream (4006 sq in.) and the discharge (417 sq in.) end of the nozzle to give $V = 8.08\sqrt{h_1 - y}$ where y was taken as 1.74 ft. Calculations were carried to the decimal places shown in order to indicate small differences responsible for a detectable change in wave pattern.

5. $h_1 = 2.58, V = 7.41, \mathbf{F}_y = 0.990, y' = 2.05$. The stable wave grows in a channel of this length (about $5.2y$) when the velocity is reduced to $\mathbf{F}_y = 1$ or below.
6. $h_1 = 2.46, V = 6.86, \mathbf{F}_y = 0.918, y' = 1.98$. The wave crest is at 3 to 3.5 ft from the nozzle exit. The depth y_D at the downstream control station is still maintained at 1.74 ft; the wave trough, however, is displaced slightly upstream where the elevation is 1.69 ft. There is some instability since h_1, y', the wave trough, and y_D fluctuate about $\pm$ 0.02 ft.
7. $h_1 = 2.32, V = 6.15, \mathbf{F}_y = 0.823, y' = 1.83$ at 3 to 3.5 ft from the nozzle exit. This pattern is stationary with the wave trough (1.69 ft. elevation) at about 7 ft from the nozzle.
8. $h_1 = 2.26, V = 5.83, \mathbf{F}_y = 0.779, y' \eqsim 1.79$. The wave pattern is unstable. From a profile with the first wave crest at its maximum (approx. 1.79 ft) elevation 3 ft and the trough 6 ft from the nozzle, the upstream slope of the second partial wave fills (advancing slightly upstream) while the first wave decreases in amplitude (while advancing downstream) until the trough is almost flattened out at an elevation higher than the nominal stream depth $y = 1.74$ ft. The depth $y_D = 1.74$ ft is momentarily exceeded. This double-peaked wave then apparently has an effective length in excess of 9 ft; its celerity consequently exceeds the velocity of the oncoming flow. The upstream peak fills in on the upstream slope; then the downstream peak rises to arrive at the initial condition of the cycle of oscillation.
9. $h_1 = 2.18, V = 5.36, \mathbf{F}_y = 0.717, y' = 1.79$. Two wave crests, one at 2 to 2.5 ft and one at 7 to 8 ft from nozzle, oscillate similar to observation 8 above.
10. $h_1 = 2.10, V = 4.85, \mathbf{F}_y = 0.648, y' = 1.80$. Wave crests reach their maximum height at 1.5 to 2 ft then at 5 to 6 ft from nozzle. The wave trough is partially filled during oscillation similar to observations 8 and 9.
11. $h_1 = 2.01, V = 4.20, \mathbf{F}_y = 0.562, y' = 1.77$. Oscillation prevents simultaneous formation of three wave crests but they develop to their sharpest and highest ($y' = 1.77$) form successively at about 1.5, 4.5 and 8 ft from the nozzle. Wave troughs drop to a minimum elevation of about 1.72 ft.
12. $h_1 = 1.98, V = 4.04, \mathbf{F}_y = 0.540, y' = 1.77$, minimum trough elevation 1.73 ft. Three waves do not use the entire 9-ft channel length but the fourth is not distinctly formed. The wave pattern is indistinct between the cycles in which the crests are successively formed.
13. $h_1 = 1.93, V = 3.52, \mathbf{F}_y = 0.471, y' = 1.76$, troughs of oscillations 1.73 ft. The length of the single wave is 2 to 2.5 ft but four waves are never formed simultaneously. This low amplitude wave pattern is indistinct and changeable.

During and soon after velocity changes, especially in an upward direction, waves reach amplitudes as much as 50 per cent higher (trough to crest) than those recorded above. The presence of a model also causes higher amplitudes and tends to anchor some of the multiple-peak patterns and partially suppress the oscillation described above.

When the channel length was reduced to 7 ft (about $4y$) observations were made in sequence as follows:

1. $h_1 = 2.39, V = 6.52, \mathbf{F}_y = 0.871, y' = 1.89$. This velocity was slowly approached in order to allow time for waves to grow.
2. $h_1 = 2.41, V = 6.61, \mathbf{F}_y = 0.884, y' = 1.89$. This is the highest wave attainable in the 7-ft channel without a model.
3. $h_1 = 2.43, V = 6.71, \mathbf{F}_y = 0.897, y' = 1.88$.
4. $h_1 = 2.44, V = 6.76, \mathbf{F}_y = 0.904, y' = 1.86$.
5. $h_1 = 2.46, V = 6.86, \mathbf{F}_y = 0.916, y' = 1.82$.
6. $h_1 = 2.51, V = 7.09, \mathbf{F}_y = 0.948, y' = 1.80$.
7. $h_1 = 2.53, V = 7.19, \mathbf{F}_y = 0.960, y' = 1.78$.
8. $h_1 = 2.55, V = 7.28, \mathbf{F}_y = 0.973, y' = 1.78$.
9. $h_1 = 2.60, V = 7.50, \mathbf{F}_y = 1.002, y' = 1.77$.

   In observations 3 to 9, the wave is stable in form. Its elevation at the crest is reduced to a negligible amount as $\mathbf{F}_y = 1$ is approached.
10. $h_1 = 2.65, V = 7.71, \mathbf{F}_y = 1.031, y' = 1.76$. Due to friction in the channel, the elevation at the center of the channel is not reduced below 1.76 ft even at higher Froude numbers.
11. $h_1 = 2.55, V = 7.28, \mathbf{F}_y = 0.973, y' = 1.78$.
12. $h_1 = 2.45, V = 6.81, \mathbf{F}_y = 0.911, y' = 1.83$.
13. $h_1 = 2.40, V = 6.57, \mathbf{F}_y = 0.878, y' = 1.87$.
14. $h_1 = 2.39, V = 6.52, \mathbf{F}_y = 0.871, y' = 1.87$.

    The stable wave grows as the Froude number is reduced. Its maximum elevation is again reached at $\mathbf{F}_y \eqsim 0.88$.
15. $h_1 = 2.32, V = 6.16, \mathbf{F}_y = 0.823, y' = 1.87$. Fluctuation of $y' = +\ 0.0 - 0.04$.

16. $h_1 = 2.26, V = 5.83, \mathbf{F}_y = 0.779, y' = 1.82$. The fluctuation continues with wave crest 2.5 ft from the new nozzle exit.
17. $h_1 = 2.20, V = 5.48, \mathbf{F}_y = 0.732, y' = 1.79$. The fluctuation continues.
18. $h_1 = 2.16, V = 5.24, \mathbf{F}_y = 0.700, y' = 1.78$. The fluctuation is similar to that of observation 8 for the 9-ft channel.
19. $h_1 = 2.07, V = 4.64, \mathbf{F}_y = 0.621, y' = 1.77$. Two wave crests have appeared with the trough at a minimum distance of 3 ft from the nozzle exit.
20. $h_1 = 2.04, V = 4.43, \mathbf{F}_y = 0.592, y' = 1.78$.
21. $h_1 = 2.00, V = 4.14, \mathbf{F}_y = 0.551, y' = 1.79$.
    Waves form in succession then coalesce into one long wave of indefinite shape.
22. $h_1 = 1.93, V = 3.52, \mathbf{F}_y = 0.471, y' = 1.76$. There is a suggestion of three waves forming in succession.

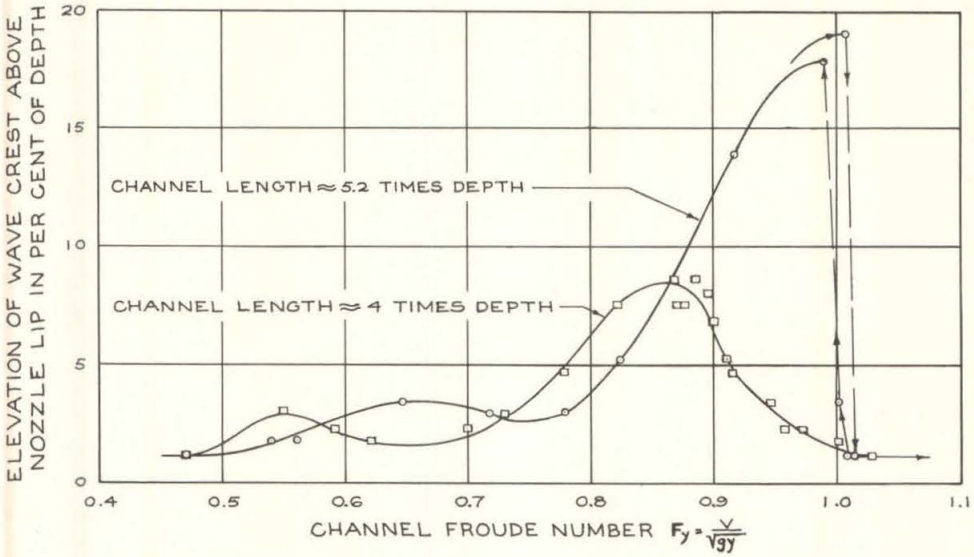

Fig. 8—Amplitude of Gravity Waves in a Free-Surface Water Tunnel

A dimensionless representation of the measured wave amplitudes for the 7- and 9-ft channel lengths is plotted in Fig. 8. The amplitudes plotted are given by $100\ (y' - y)/y$ where y' is the surface elevation of the wave crest and y is the surface elevation at the nozzle and at the downstream control station.

The waves in the longer channel reach an amplitude of about 18 per cent of the depth at a channel Froude number, $\mathbf{F}_y = V/\sqrt{gy} \approx 1$. The wave persists as the velocity is increased to produce a Froude number slightly greater than 1.0. After reaching sufficient velocity to sweep the wave out of the channel, the Froude number must be reduced to 1.0 or slightly less before the large wave will grow again. This is indicated by the dotted lines and arrows in Fig. 8. The waves in the shorter channel reach a maximum amplitude of only about 8 per cent of the depth when the Froude number is about 0.86. As the velocity is increased, the wave amplitude gradually decreases and becomes quite small before a Froude number of 1.0 is reached.

The slight elevation that persists at Froude numbers above 1.0 might be attributed to the effects of channel friction and possibly to slight curvature of flow near the nozzle exit. The original observation notes indicate that the intermediate wave troughs were often lower than the trough at the nozzle lip. This occurred at low Froude numbers where low points occur on the curves of wave-crest elevation in Fig. 8. Maximum trough-to-crest amplitudes in this zone are consequently higher than indicated by the elevation relative to the nozzle lip.

It was difficult to accurately measure the length of the waves. The maximum length of the single primary gravity wave of large amplitude is not expected to greatly exceed the length of the working section since the control stations at the nozzle lip and diffuser entrance are kept at the same depth ($y = 1.74$ ft) and these stations correspond approximately with the wave troughs. There is considerable uncertainty in the length estimates when the amplitude is small enough for points on the wave profile other than the trough to be located at the downstream control station. Furthermore, the above data show that the length is not constant at the lower Froude numbers where the waves definitely are not of permanent type.

It appears that waves will be formed in a free-surface water tunnel at any velocity below that required to sweep the longest wave downstream and out of the open channel. As the velocity is reduced below the value required to hold the highest wave in the working section, the wave amplitude and length will be reduced a sufficient amount for the celerity of the disturbance to continue to be equal to the stream velocity. Although this mechanism provides some disturbance at all low Froude numbers, the use of a short working section will reduce the amplitudes attained as well as the range of channel Froude numbers which produce wave amplitudes high enough to prevent satisfactory operation.

APPENDIX II

Preparation of the Dynamic-Similitude Chart

With Froude number as abscissa and model or prototype length as ordinate, the coordinates of points on lines of constant velocity, Weber number, and Reynolds number are obtained by expressing the relationship between length and Froude number in terms of the significant fluid properties and the respective chosen constant conditions. The Froude number $\mathbf{F} = V/\sqrt{gl}$ can be rearranged as

$$l = \frac{V^2}{g}\frac{1}{\mathbf{F}^2} \qquad (1)$$

in order to show the desired relationship when a constant velocity is chosen. The Weber number $\mathbf{W} = V/\sqrt{\sigma/\rho l}$ rearranged as $V = \mathbf{W}\sqrt{\sigma/\rho l}$ and substituted for the velocity gives

$$l = \mathbf{W}\sqrt{\frac{\sigma}{\rho g}}\frac{1}{\mathbf{F}} \qquad (2)$$

as the relationship involving Weber number and the significant constant fluid properties. In a similar manner, the Reynolds number $\mathbf{R} = Vl/\nu$ combines with equation (1) to produce

$$l^3 = \frac{\mathbf{R}^2\nu^2}{g}\frac{1}{\mathbf{F}^2}$$

or

$$l = \left(\frac{\mathbf{R}\nu}{\sqrt{g}}\right)^{2/3}\frac{1}{\mathbf{F}^{2/3}}. \qquad (3)$$

Since equations (1), (2), and (3) are in powers of l and $\mathbf{F}$, the chosen constant conditions plot as straight lines on log-log paper. By use of these equations and the water properties indicated on the face of the similitude chart (Fig. 3), the coordinates of points are found that establish the position of the desired lines. For a constant velocity of 100 fps, the points ($\mathbf{F} = 17.6$, $l = 1$) and ($\mathbf{F} = 1.76$, $l = 100$) can be used. For $V = 50$ fps, ($\mathbf{F} = 8.8$, $l = 1$) and ($\mathbf{F} = 0.88$, $l = 100$) determine the line and for $V = 20$ fps, ($\mathbf{F} = 3.52$, $l = 1$) and ($\mathbf{F} = 0.352$, $l = 100$) are sufficient. A line representing a constant Weber number of 10^3 contains the points ($\mathbf{F} = 0.1$, $l = 89.8$) and ($\mathbf{F} = 10$, $l = 0.898$); the points ($\mathbf{F} = 0.1$, $l = 166$) and ($\mathbf{F} = 10$, $l = 7.7$) locate the line of constant Reynolds number $\mathbf{R} = 10^8$. Since Froude number is to the same power as velocity, Weber number, and Reynolds number in equations (1), (2), and (3), the lines representing decade intervals repeat at the same abscissa spacing as a decade on the Froude-number scale.

The use of the similitude chart is described on page 4 and illustrated in Figs. 3 to 6. The chart is reproduced as a transparency in the frontispiece for the convenience of those who wish to reproduce it for their own use.

Distribution List

for

"HYDRODYNAMICS OF THE FREE-SURFACE WATER TUNNEL"

Report No. N-65

COPY NO.	NAME AND ADDRESS
15	Office of Naval Research, Department of the Navy, Washington 25, D.C., Attn: Fluid Mech. Br. (Code 426)
1	Commanding Officer, Branch Office, U.S. Navy Office of Naval Research, 495 Summer Street, Boston 10, Massachusetts
1	Commanding Officer, Branch Office, U.S. Navy Office of Naval Research, 50 Church Street, New York 7, N.Y.
1	Commanding Officer, Branch Office, U.S. Navy Office of Naval Research, 844 North Rush Street, Chicago 11, Illinois
1	Commanding Officer, Branch Office, U.S. Navy Office of Naval Research, 801 Donahue Street, San Francisco 24, California
2	Commanding Officer, Branch Office, U.S. Navy Office of Naval Research, 1030 East Green Street, Pasadena 1, California
2	Assistant Naval Attache for Research, U.S. Navy Office of Naval Research, American Embassy, London, England, Navy 100, F.P.O. New York, N.Y.
1	Naval Research Laboratory, U.S. Navy Office of Naval Research, Washington 20, D.C., Attn: Librarian (Code 2021)
1	Executive Secretary, Research and Development Board, National Defense Building, Washington, D.C.
1	Bureau of Aeronautics, Department of the Navy, Washington 25, D.C., Attn: Aero and Hydro Branch (Code De3)
1	Bureau of Ordnance, Department of the Navy, Washington 25, D.C. Attn: Code Re2c
1	Bureau of Ordnance, Department of the Navy, Washington 25, D.C. Attn: Code Re3d
1	Bureau of Ordnance, Department of the Navy, Washington 25, D.C. Attn: Code Re6a
2	Bureau of Ordnance, Department of the Navy, Washington 25, D.C. Attn: Code Re9
5	Bureau of Ordnance, Department of the Navy, Washington 25, D.C. Attn: Code Ad3
1	Naval Ordnance Laboratory, U.S. Navy Bureau of Ordnance, White, Oak, Silver Spring 19, Md., Attn: Dr. R.J. Seeger
3	Underwater Ordnance Division, Naval Ordnance Test Station, 3202 E. Foothill Blvd., Pasadena, California
1	Bureau of Ships, Department of the Navy, Washington 25, D.C., Attn: Research Division (Code 372)
3	David Taylor Model Basin, Department of the Navy, Washington 7, D.C., Attn: Hydromechanics Department
1	Department of the Army, General Staff, National Defense Building, Washington, D.C., Attn: Director of Research and Development
1	Commanding Officer, Army Chemical Center, Chemical Corps, Procurement Agency, Medical Division, Edgewood Md., Attn: Dr. F.A. Odell
1	Ballistic Research Laboratories, Department of the Army, Aberdeen Proving Ground, Maryland, Attn: Mr. R.H. Kent
1	Director of Research, National Advisory Committee for Aeronautics, 1724 F. Street, N.W., Washington, D.C.
1	Director, Langley Aeronautical Laboratory, National Advisory Committee for Aeronautics, Langley Field, Virginia
1	Dr. J.H. Wayland, Division of Civil and Mechanical Eng. and Aeronautics, California Institute of Technology, Pasadena, California
1	Professor G. Birkhoff, Dept. of Mathematics, Harvard University, 576 Widener Library, Cambridge 38, Massachusetts
1	Dr. K.S.M. Davidson, Experimental Towing Tank, Stevens Inst. of Technology, Hoboken, New Jersey
1	Dr. J.H. McMillen, Naval Ordnance Laboratory, Naval Gun Factory, Washington 25, D.C.
1	Dr. F.A. Maxfield, Bureau of Ordnance (Code Re6a), Department of the Navy, Washington 25, D.C.

1	Dr. A. Miller, Bureau of Ordnance (Code Re3d), Department of the Navy, Washington 25, D.C.
1	Dr. H. Rouse, Iowa Institute of Hydraulic Research, State University of Iowa, Iowa City, Iowa
1	Dr. J.V. Wehausen, Hydromechanics Department, David Taylor Model Basin, Department of the Navy, Washington, D.C.
1	University of California, Engineering Research Projects, Berkeley 4, California, Attn: Dr. R.G. Folsom
1	University of California, Department of Engineering, Los Angeles 24, California. Attn: Prof. L.B. Slichter
1	University of Chicago, Chicago, Illinois, Attn: Dr. T.E. Caywood
1	Columbia University, Department of Civil Engineering, New York 27, N.Y. Attn: Professor B.A. Bakhmeteff
1	Illinois Institute of Technology, Department of Fundamental Mechanics Research, Chicago 16, Illinois, Attn: Professor V.L. Streeter
1	Indiana University, Department of Mathematics, Bloomington, Indiana Attn: Dr. D. Gilbarg
1	The Johns Hopkins University, Mechanical Engineering Department, Baltimore, Maryland, Attn: Dr. G.F. Wislicenus
1	Massachusetts Institute of Technology, Department of Civil and Sanitary Engineering, Cambridge 39, Massachusetts, Attn: Dr. A. T. Ippen
1	University of Michigan, Engineering Mechanics Department, Ann Arbor, Michigan, Attn: Professor R.A. Dodge
1	St. Anthony Falls Hydraulic Laboratory, University of Minnesota, Minneapolis 14, Minnesota, Attn: Dr. L.G. Straub
1	New York University, Institute for Mathematics and Mechanics, 45 Fourth Avenue, New York 3, New York, Attn: Dr. J.J. Stoker
1	Northwestern University, Department of Civil Engineering, Evanston, Illinois, Attn: Prof. W.S. Hamilton
1	University of Notre Dame, College of Engineering, Notre Dame, Indiana, Attn: Prof. K.E. Schoenherr
1	Director, The Pennsylvania State College, School of Engineering, Ordnance Research Laboratory, State College, Pennsylvania
1	Society of Naval Architects and Marine Engineers, 29 West 39 St., New York City., N.Y.
1	University of Southern California, Department of Physics, Los Angeles, California, Attn: Dr. R.E. Vollrath
1	Stanford University, Department of Civil Engineering, Stanford, California, Attn: Prof. J.K. Vennard
1	Stanford University, Department of Physics, Stanford, California, Attn: Dr. L.I. Schiff.
1	Woods Hole Oceanographic Institute, Woods Hole, Massachusetts, Attn: Dr. Columbus Iselin.
1	Worcester Polytechnic Institute, Alden Hydraulic Laboratory, Worcester, Mass.; Attn: Prof. J.L. Hooper
2	Commanding Officer, Naval Torpedo Station, Newport, Rhode Island
2	Commander, Naval Ordnance Laboratory, White Oak, Silver Spring 19, Md.
2	Commander, Naval Ordnance Test Station, Inyokern, China Lake, Calif.
1	Inspector of Naval Material, 1206 South Santee Street, Los Angeles, 15, California
2	Superintendent, U.S. Navy Postgraduate School, Annapolis, Maryland
2	Director, U.S. Naval Electronics Laboratory, Point Loma, San Diego, California
2	Research Analysis Group, National Research Council, 2101 Constitution Avenue, Washington, D.C.
10	British Joint Services Mission (Navy Staff) 1910 K Street, N.W., Washington, D.C.